A Quasi-Planar Model for Gravity-Capillary Interfacial Waves in Deep Water

By Z. Wang, J.-M. Vanden-Broeck and H. Meng*

A dynamical model equation for interfacial gravity-capillary waves between two semi-infinite fluid layers, with a lighter fluid lying above a heavier one, is derived. The model proposed is based on the fourth-order truncation of the kinetic energy in the Hamiltonian of the full problem, and on weak transverse variations, in the spirit of the Kadomtsev-Petviashvilli equation. It is well known that for the interfacial gravity-capillary waves in deep water, there is a critical density ratio where the associated cubic nonlinear Schrödinger equation changes type. Our numerical results reveal that, when the density ratio is below the critical value, the bifurcation diagram of plane solitary waves behaves in a way similar to that of the free-surface gravity-capillary waves on deep water. However, the bifurcation mechanism in the vicinity of the minimum of the phase speed is essentially similar to that of free-surface gravity-flexural waves on deep water, when the density ratio is in the supercritical regime. Different types of lump solitary waves, which are fully localized in both transverse and longitudinal directions, are also computed using our model equation. Some dynamical experiments are carried out via a marching-in-time algorithm.

1 Introduction

Interfacial waves play an important role in transferring heat, energy, and momentum in geophysical fluids. Some fundamental problems in fluid dynamics, including the onset mechanism of wind ripples, and the origin, propagation and spatial distribution of large internal waves in both the ocean and the atmosphere due to the natural density stratification, can be modeled by a fluid geometry composed by two immiscible fluid layers with different densities. Over the last

*Address for correspondence: Zhan Wang, Department of Mathematics, University College London, London, WC1E 6BT, UK; email: zhan.wang@ucl.ac.uk

few decades interfacial waves have been intensively investigated theoretically, experimentally and numerically. From the point of view of weakly nonlinear theory, the celebrated Korteweg-de Vries (KdV) equation is commonly used when both layers are shallow compared to the typical wavelength. This is then denoted as the shallow-shallow case (the reader is referred to the comprehensive review paper by Helfrich & Melville [10]). Under the assumption of the upper layer being thin but the lower layer being thick compared to the characteristic wavelength, the evolution of the interface is governed by the Benjamin-Ono (BO) equation, which is referred to as the shallow-deep case. A great deal of work has been achieved on internal waves in both the shallow-shallow and the shallow-deep cases. In this paper, we propose a dynamic model equation for the interfacial gravity-capillary (GC) waves in the deep-deep case, where both layers are supposed to be infinitely deep.

For a two-dimensional fluid geometry (corresponding to a one-dimensional interface or a one-dimensional free surface and henceforth denoted as "1D problem" or "plane waves"), it is well known that both the KdV and the BO equations have soliton solutions decaying monotonically to zero in space. In contrast to these "long" solitons, a new type of solitary waves with decaying oscillatory tails, which are usually called wavepacket solitary waves, have been found in surface water wave problems when the effects of surface tension are taken into account. It is known that the existence of wavepacket solitary wave demands a global extremum in the linear dispersion relation at finite wavenumber where the group velocity (i.e. the velocity at which the envelop of the waves propagates) and the phase velocity (i.e. the velocity at which the crest of each wave travels) are equal. An additional condition for the existence of wavepacket solitary waves bifurcating from infinitesimal periodic waves is that the associated cubic nonlinear Schrödinger (NLS) equation (which governs the small-amplitude and slowly-varying envelope of a monochromatic carrier wave at that extremum) is of focusing type. A typical example that satisfies these two conditions is the free-surface GC solitary waves on deep water.

However, when the second condition is not satisfied (i.e. the associated cubic NLS is of defocusing type), some water wave problems can still support wavepacket solitary waves. A typical example is the interfacial GC waves in deep water. This is the problem that we address in this paper. Under proper non-dimensionalization (see §2.1), the linear dispersion relation for the problem considered takes the form

$$\omega^2 = \frac{|k|}{1+R}\left(1 - R + k^2\right), \qquad c_p = \frac{\omega}{k} = \sqrt{\frac{1}{1+R}\left[\frac{1-R}{|k|} + |k|\right]} \tag{1}$$

where ω is the wave frequency, k is the wavenumber, c_p is the phase velocity, and $R < 1$ is the density ratio of the upper layer to the lower layer. It is obvious that, for each fixed R, c_p has a global minimum $c_p^* = \sqrt{\frac{2\sqrt{1-R}}{1+R}}$ at the critical wavenumber $k^* = \sqrt{1-R}$. Dias & Iooss [8] performed a normal form analysis

at this critical point resulting in the cubic NLS equation

$$iA_\tau + \lambda(R)\, A_{XX} + \mu(R)\, \left|A\right|^2 A = 0 \tag{2}$$

where the coefficients λ and μ both depend on the density ratio. Since the carrier wave that we are interested in is at the minimum of the dispersion relation, $\lambda(R) = \frac{\omega''}{2}(k^*, R)$ is positive definite. However, the nonlinear coefficient $\mu(R)$, the only term that determines the type of the cubic NLS, changes sign at the critical density ratio $R_c \approx 0.283$. More precisely, if $0 < R < R_c$ the cubic NLS is of focusing type and has sech-type bright soliton solutions, while if $R_c < R < 1$ the NLS is defocusing and tanh-type dark solitons can be expected. Nevertheless, Laget & Dias in [13] show that wavepacket solitary waves can exist as solutions of the irrotational Euler equations for all $0 < R < 1$, even when the underlying cubic NLS is of defocusing type. Their numerical results demonstrate that, above the critical density ratio, the solitary waves are unusual, since they can only exist with finite amplitudes. In other words, they bifurcate neither from infinitesimal periodic waves like the free-surface GC waves on deep water, nor from infinitesimal long waves like the solutions of the KdV equation. Therefore, the completed bifurcation digram of the interfacial GC solitary waves for the supercritical density ratio is not fully understood.

The recent research on the free-surface gravity-flexural (GF) waves, a problem seemingly unrelated, shed light on the study of the bifurcation mechanism of the interfacial GC waves in deep water. The GF wave problem, with the curvature term due to surface tension in the Bernoulli equation replaced by a term containing the second derivative of the curvature, has been proposed as a model for wave propagation under floating ice sheet (see Milewski *et al.* [14] and references therein). For the GF waves on a fluid of arbitrary depth, the associated cubic NLS equation is of defocusing type when the mean depth of the fluid is greater than a critical value. In spite of this, Milewski *et al.* [14] show that solitary waves still occur in deeper water, but they are a new type in the sense that they occur along a branch of generalized solitary waves that itself bifurcates from periodic waves of finite amplitude. In this paper, our numerical results based on our reduced model equation reveal a similar bifurcation mechanism for the interfacial GC solitary waves in deep water when the density ratio is in the supercritical regime.

For a three-dimensional fluid domain (with a two-dimensional free surface or interface and henceforth denoted as "2D problem"), fully localized GC solitary waves, which are referred to as "lumps", have been shown to exist in a fluid of arbitrary depth. This is to be contrasted with the problem of pure gravity waves where solitary waves exist only in 1D problem and only in the shallow water regime (see the rigorous proof in Craig [5]). For the 2D GC interfacial solitary waves in deep water, Părău *et al.* [16] use a boundary integral method to show that lumps can exist for the irrotational Euler system even when $R > R_c$. This is similar to the 1D case. However accurate solutions for 2D steady and unsteady waves with the Euler equations are computationally expensive and difficult to obtain because of the large number of grid points needed. Therefore

it is beneficial to work with a reduced model satisfying minimal assumptions in order to obtain a better understanding of the dynamics of the interfacial GC waves. We extend our 1D model to 2D in the spirit of the Kadomtsev-Petviashvili equation, where only the slow variations of the wave in the direction transverse to the direction of propagation are considered. Our model captures two main wavepacket solitary waves: depression and elevation lumps, which have already been found in the Euler system, and high-energy solitary waves with more complicated wave patterns .

The rest of the paper is structured as follows. In section 2 we formulate mathematically the interfacial GC wave problem in deep water and derive our main model using the fourth-order truncation of the kinetic energy in the Hamiltonian expression of the full problem. In section 3 we briefly describe how to derive the associated NLS from our model system which is consistent with that derived from the primitive Euler equation. In section 4, the 1D problem near the bifurcation point is carefully investigated for both $R < R_c$ and $R > R_c$. In particular for the latter case, we show that the bifurcation diagram in the vicinity of the minimum of the phase speed is composed of Stokes, bright solitary, generalized solitary, and dark solitary waves. Then numerical results for the 2D problem are shown in section 5, including the existence of traveling lump solutions and their dynamics. Lastly, some concluding remarks and extensions are presented in section 6.

2 Derivation

2.1 Mathematical Formulation

Consider a three-dimensional incompressible, inviscid and irrotational flow, composed by two immiscible layers with the lighter one lying above the heavier one. The upper layer (denoted by D^+) and the lower layer (denoted by D^-) are both supposed to be semi-infinite and separated by a sharp interface $z = \eta(x, y, t)$, where x is the wave propagating direction, y is the transverse direction and the $z-$axis points upwards with $z = 0$ at the undisturbed interface. The constant densities in D^+ and D^- are denoted by ρ^+ and ρ^- respectively, therefore $\rho^+ < \rho^-$. The velocity potential in each layer satisfies Laplace equation

$$\Delta\phi^- + \phi^-_{zz} = 0, \qquad \text{for } z < \eta(x, y, t)$$
$$\Delta\phi^+ + \phi^+_{zz} = 0, \qquad \text{for } z > \eta(x, y, t)$$

where $\Delta = \partial_{xx} + \partial_{yy}$ is the two-dimensional operator acting in the horizontal variables. On the interface $z = \eta(x, y, t)$, the nonlinear kinematic and dynamic

boundary conditions read:

$$\eta_t = \phi_z^- - \nabla\phi^- \cdot \nabla\eta = \phi_z^+ - \nabla\phi^+ \cdot \nabla\eta, \tag{3}$$

$$\rho^-\phi_t^- - \rho^+\phi_t^+ + \frac{\rho^-}{2}\left[\left|\nabla\phi^-\right|^2 + (\phi_z^-)^2\right] - \frac{\rho^+}{2}\left[\left|\nabla\phi^+\right|^2 + (\phi_z^+)^2\right]$$
$$+(\rho^- - \rho^+)g\eta - \sigma\nabla\cdot\left[\frac{\nabla\eta}{\sqrt{1+|\nabla\eta|^2}}\right] = 0 \tag{4}$$

where ∇ and $\nabla\cdot$ are the gradient and divergent operators respectively, acting in the horizontal variables, g is the acceleration of gravity and σ is the surface tension coefficient. Since both gravity and surface tension are considered in this paper, one can non-dimensionalize the system by choosing

$$\left[\frac{\sigma}{\rho^- g}\right]^{1/2}, \quad \left[\frac{\sigma}{\rho^- g^3}\right]^{1/4} \quad \text{and} \quad \left[\frac{\sigma^3}{(\rho^-)^3 g}\right]^{1/4} \tag{5}$$

as length, time and potential scales respectively. Therefore the dynamic boundary condition (4) can be reduced to

$$\phi_t^- - R\phi_t^+ + \frac{1}{2}\left[\left|\nabla\phi^-\right|^2 + (\phi_z^-)^2\right] - \frac{R}{2}\left[\left|\nabla\phi^+\right|^2 + (\phi_z^+)^2\right]$$
$$+(1-R)\eta - \nabla\cdot\left[\frac{\nabla\eta}{\sqrt{1+|\nabla\eta|^2}}\right] = 0 \tag{6}$$

where $R = \frac{\rho^+}{\rho^-} < 1$ is the density ratio. Furthermore, the kinematic boundary condition (3) implies that the normal velocity of the fluid is continuous across the interface

$$\left(\phi_x^-, \phi_y^-, \phi_z^-\right)^\top \cdot \mathbf{n} = \left(\phi_x^+, \phi_y^+, \phi_z^+\right)^\top \cdot \mathbf{n} \tag{7}$$

where $\mathbf{n} = \frac{1}{\sqrt{1+\eta_x^2+\eta_y^2}}(-\eta_x, -\eta_y, 1)^\top$ is the unit normal vector pointing upwards on the interface. Finally, the boundary condition at infinity

$$\phi_z^\pm \to 0 \quad \text{as} \quad z \to \pm\infty \tag{8}$$

completes the whole system.

2.2 Hamiltonian and Truncation

The classic surface water wave problem can be written in a canonical form in the sense of Zakharov [21], which is also true for two-layer interfacial waves (see Benjamin & Bridges [3]). We can write the Hamiltonian for interfacial waves as

the total energy:

$$\begin{aligned}\mathcal{H}\left[\phi^{\pm},\eta\right] &= \frac{1}{2}\int_{\mathbb{R}^2}\int_{-\infty}^{\eta}\left[\left|\nabla\phi^{-}\right|^2+\left(\phi_z^{-}\right)^2\right]dz\,dxdy+\\ &\quad \frac{R}{2}\int_{\mathbb{R}^2}\int_{\eta}^{+\infty}\left[\left|\nabla\phi^{+}\right|^2+\left(\phi_z^{+}\right)^2\right]dz\,dxdy+\\ &\quad \frac{1-R}{2}\int_{\mathbb{R}^2}\eta^2\,dxdy+\int_{\mathbb{R}^2}\left(\sqrt{1+|\nabla\eta|^2}-1\right)dxdy. \qquad (9)\end{aligned}$$

The most important term in the Hamiltonian formulation of the free-surface water wave problem is called the Dirichlet to Neumann operator (DNO) which maps the Dirichlet boundary condition to normal derivatives on the boundary via solving Laplace equation. If we define the surface velocity potentials as $\xi^{\pm}(x,y,t)\triangleq\phi^{\pm}(x,y,\eta(x,y,t),t)$, then the Dirichlet to Neumann operators $G^{\pm}$, which are associated with the kinematic boundary conditions, are of the forms

$$\eta_t = G^{-}(\eta)\xi^{-} = \left(\phi_x^{-},\phi_y^{-},\phi_z^{-}\right)^{\top}\cdot\mathbf{n}\,\sqrt{1+|\nabla\eta|^2} \qquad (10)$$

$$\eta_t = -G^{+}(\eta)\xi^{+} = -\left(\phi_x^{+},\phi_y^{+},\phi_z^{+}\right)^{\top}\cdot\left(-\mathbf{n}\right)\sqrt{1+|\nabla\eta|^2}. \qquad (11)$$

Following Benjamin & Bridges [3], we introduce $\phi=\phi^{-}-R\phi^{+}$ and $\xi=\xi^{-}-R\xi^{+}$. It follows from (10)–(11) that

$$G^{+}\xi = \left(G^{+}+RG^{-}\right)\xi^{-} \implies \xi^{-} = \left(G^{+}+RG^{-}\right)^{-1}G^{+}\xi. \qquad (12)$$

Using the divergence theorem and (12), one can rewrite the Hamiltonian (9) in terms of ξ and η as

$$\begin{aligned}\mathcal{H}[\xi,\eta] &= \frac{1}{2}\int_{\mathbb{R}^2}\left(\xi^{-}\frac{\partial\phi^{-}}{\partial\mathbf{n}}-R\xi^{+}\frac{\partial\phi^{+}}{\partial\mathbf{n}}\right)_{z=\eta}\sqrt{1+|\nabla\eta|^2}\,dxdy+\\ &\quad \frac{1-R}{2}\int_{\mathbb{R}^2}\eta^2\,dxdy+\int_{\mathbb{R}^2}\left(\sqrt{1+|\nabla\eta|^2}-1\right)dxdy\\ &= \frac{1}{2}\int_{\mathbb{R}^2}\xi G^{-}\left(G^{+}+RG^{-}\right)^{-1}G^{+}\xi\,dxdy+\\ &\quad \frac{1-R}{2}\int_{\mathbb{R}^2}\eta^2\,dxdy+\int_{\mathbb{R}^2}\left(\sqrt{1+|\nabla\eta|^2}-1\right)dxdy. \qquad (13)\end{aligned}$$

Therefore the canonical form of the Hamiltonian takes the form

$$\eta_t = \frac{\delta\mathcal{H}}{\delta\xi}, \qquad \xi_t = -\frac{\delta\mathcal{H}}{\delta\eta}. \qquad (14)$$

Coifman and Meyer [7] proved that if the C^1-norm of η is smaller than a certain constant, then $G^{\pm}$ are analytic functions of η. It follows that the DNO can be

naturally written in the form of the Taylor expansion $G^{\pm} = \sum G_i^{\pm}$. For the lower half plane, the first three terms of the Taylor series of the DNO are given by

$$G_0^-(\eta) = \big(-\Delta\big)^{1/2} \tag{15}$$

$$G_1^-(\eta) = -G_0\eta G_0 - \nabla\cdot\eta\nabla \tag{16}$$

$$G_2^-(\eta) = \frac{1}{2}\Delta\eta^2 G_0 + \frac{1}{2}G_0\eta^2\Delta + G_0\eta G_0\eta G_0. \tag{17}$$

It is noted that the DNO in the upper half plane can be expanded as

$$G^+(\eta) = \sum_{j=0}^{\infty}(-1)^j G_j^-(\eta) \tag{18}$$

which is derived by replacing η with $-\eta$ in each $G_j^-(\eta)$. Therefore we can suppress the superscript "$-$" in (15)-(17) for simplicity. Now we start to derive a quartic-Hamiltonian-truncation model. For this purpose, the key point is to Taylor expand the pseudo-differential operator closely related to the kinetic energy in the Hamiltonian (13). Following Craig & Groves [6], we have

$$G^-\big(G^+ + RG^-\big)^{-1}G^+ = \frac{1}{1+R}G_0 + \frac{1-R}{(1+R)^2}G_1 + \frac{1}{1+R}G_2$$

$$-\frac{4R}{(1+R)^3}G_1G_0^{-1}G_1 + O\big(|\eta|^3\big). \tag{19}$$

When $R=0$, the expression (19) reduces to the one-layer case, which has been used in [20] to investigate extensively the dynamics of the 2D free-surface GC solitary waves.

In this paper, we consider waves that are slightly inhomogeneous in the transverse direction (y direction), i.e., the wave propagation direction is not far from the x direction. Therefore in the spirit of the Kadomtsev-Petviashvili (KP) equation, we keep the linear part of the model equation exactly the same as that of the primitive irrotational Euler equation, but leave the nonlinear terms y-independent. For this purpose, we introduce

$$\widetilde{G}_0(\eta) = \big(-\partial_{xx}\big)^{1/2} \tag{20}$$

$$\widetilde{G}_1(\eta) = -\widetilde{G}_0\eta\widetilde{G}_0 - \partial_x\eta\partial_x \tag{21}$$

$$\widetilde{G}_2(\eta) = \frac{1}{2}\partial_{xx}\eta^2\widetilde{G}_0 + \frac{1}{2}\widetilde{G}_0\eta^2\partial_{xx} + \widetilde{G}_0\eta\widetilde{G}_0\eta\widetilde{G}_0. \tag{22}$$

Neglecting the $O(|\eta|^3)$ terms and treating the expression in the KP sense, (19) can be approximated by

$$\widetilde{G} = \frac{1}{1+R}G_0 + \frac{1-R}{(1+R)^2}\widetilde{G}_1 + \frac{1}{1+R}\widetilde{G}_2 - \frac{4R}{(1+R)^3}\widetilde{G}_1\widetilde{G}_0^{-1}\widetilde{G}_1. \tag{23}$$

Noting that $\partial_x \widetilde{G}_0^{-1} \partial_x = -\widetilde{G}_0$, we obtain

$$\widetilde{G}_1 \widetilde{G}_0^{-1} \widetilde{G}_1 = \widetilde{G}_0 \eta \widetilde{G}_0 \eta \widetilde{G}_0 + \widetilde{G}_0 \eta \partial_x \eta \partial_x + \partial_x \eta \partial_x \eta \widetilde{G}_0 - \partial_x \eta \widetilde{G}_0 \eta \partial_x. \tag{24}$$

Using (23), the Hamiltonian (13) can be approximated by

$$\widetilde{\mathcal{H}}[\xi, \eta] = \frac{1}{2} \int \xi \widetilde{G} \xi \, dxdy + \frac{1-R}{2} \int \eta^2 \, dxdy + \int \left(\sqrt{1 + |\nabla \eta|^2} - 1 \right) dxdy. \tag{25}$$

Finally, by taking the variational derivatives as (14), after tedious but straightforward calculations, we obtain a reduced model system for the following quasi-planar interfacial gravity-capillary waves in deep water

$$\begin{bmatrix} \partial_t & -\frac{1}{1+R} G_0 \\ (1-R) - \Delta & \partial_t \end{bmatrix} \begin{pmatrix} \eta \\ \xi \end{pmatrix} = \begin{bmatrix} \mathcal{N}_1(\xi, \eta) \\ \mathcal{N}_2(\xi, \eta) \end{bmatrix} \tag{26}$$

where

$$\mathcal{N}_1 = \frac{1-R}{(1+R)^2} \widetilde{G}_1 \xi + \frac{1}{1+R} \widetilde{G}_2 \xi - \frac{4R}{(1+R)^3} \widetilde{G}_1 \widetilde{G}_0^{-1} \widetilde{G}_1 \xi \tag{27}$$

$$\begin{aligned} \mathcal{N}_2 = {} & \frac{1-R}{2(1+R)^2} \left[\left(\widetilde{G}_0 \xi \right)^2 - \left(\partial_x \xi \right)^2 \right] - \frac{1}{1+R} \left(\widetilde{G}_0 \xi \right) \left(\widetilde{G}_0 \eta \widetilde{G}_0 \xi + \eta \partial_{xx} \xi \right) \\ & + \frac{4R}{(1+R)^3} \left[\left(\widetilde{G}_0 \xi \right) \left(\widetilde{G}_0 \eta \widetilde{G}_0 \xi + \partial_x \eta \partial_x \xi \right) + \left(\partial_x \xi \right) \left(\widetilde{G}_0 \eta \partial_x \xi - \partial_x \eta \widetilde{G}_0 \xi \right) \right] \\ & + \partial_x \left[\frac{\eta_x}{\sqrt{1 + |\nabla \eta|^2}} - \eta_x \right] + \partial_y \left[\frac{\eta_y}{\sqrt{1 + |\nabla \eta|^2}} - \eta_y \right]. \end{aligned} \tag{28}$$

The KP approximation is generally applied to the uni-directional nearly plane waves (see, for example, Akers & Milewski [2] and Kim & Akylas [11]). We use the same approximation in this paper. It should be noted that the formulae (19) and (24) are not new. To the best of our knowledge the second term in the right-hand side of (19) was first calculated in [12], while the third and fourth terms were derived in [6]. In the 1D case, the high-order terms in the expression (19), which were used to derive the cubic-quintic NLS for studying the transition regime $R \approx R_c$, were provided in [1].

Since in the following sections, we choose R so that γ is not close to zero, the effects of the quintic nonlinearity can be neglected compared to that of the cubic nonlinearity in the small-amplitude limit. The rationale for the quartic Hamiltonian truncation is to guarantee at least the same local bifurcation behavior in the model and in the potential flow. Furthermore, our numerics will show that the model is still quantitatively accurate for the moderate-amplitude waves. Our numerical experiments indicate that there is not much difference between retaining the fully nonlinear interfacial tension term and treating it in the spirit of the KP equation. Therefore we keep the full interfacial tension to obtain a better energy expression.

For convenience, we recast the system (26)-(28) as a single evolution equation. Numerical experiments are implemented on a double-periodic domain, where the Fourier transform is applicable in spatial variables, hence,

$$\begin{pmatrix}\widehat{\eta}\\ \widehat{\xi}\end{pmatrix}_t + \begin{bmatrix}0 & -\frac{|\mathbf{k}|}{1+R}\\ 1-R+|\mathbf{k}|^2 & 0\end{bmatrix}\begin{pmatrix}\widehat{\eta}\\ \widehat{\xi}\end{pmatrix} = \begin{pmatrix}\widehat{\mathcal{N}}_1\\ \widehat{\mathcal{N}}_2\end{pmatrix} \tag{29}$$

where the hat indicates the Fourier transform and $\mathbf{k} = (k, l)$ is the wavenumber in Fourier space. We then multiply (29) by a matrix to diagonalize the system

$$\begin{bmatrix}1 & \frac{i|\mathbf{k}|}{(1+R)\omega}\\ 1 & \frac{-i|\mathbf{k}|}{(1+R)\omega}\end{bmatrix}\begin{pmatrix}\widehat{\eta}\\ \widehat{\xi}\end{pmatrix}_t + \begin{bmatrix}i\omega & 0\\ 0 & -i\omega\end{bmatrix}\begin{bmatrix}1 & \frac{i|\mathbf{k}|}{(1+R)\omega}\\ 1 & \frac{-i|\mathbf{k}|}{(1+R)\omega}\end{bmatrix}\begin{pmatrix}\widehat{\eta}\\ \widehat{\xi}\end{pmatrix} = \begin{bmatrix}1 & \frac{i|\mathbf{k}|}{(1+R)\omega}\\ 1 & \frac{-i|\mathbf{k}|}{(1+R)\omega}\end{bmatrix}\begin{pmatrix}\widehat{\mathcal{N}}_1\\ \widehat{\mathcal{N}}_2\end{pmatrix}. \tag{30}$$

Introducing the notation $\widehat{p} = \widehat{\eta} + \frac{i|\mathbf{k}|}{(1+R)\omega}\widehat{\xi}$ and $\widehat{q} = \widehat{\eta} - \frac{i|\mathbf{k}|}{(1+R)\omega}\widehat{\xi}$, we can rewrite the system as

$$\widehat{p}_t + i\omega\widehat{p} = \widehat{\mathcal{N}}_1 + \frac{i|\mathbf{k}|}{(1+R)\omega}\,\widehat{\mathcal{N}}_2 \tag{31}$$

$$\widehat{q}_t - i\omega\widehat{q} = \widehat{\mathcal{N}}_1 - \frac{i|\mathbf{k}|}{(1+R)\omega}\,\widehat{\mathcal{N}}_2. \tag{32}$$

Using the fact that ξ and η are both real, these two equations are eventually equivalent, and ξ and η can be recovered from p alone with

$$\widehat{\eta} = \frac{1}{2}\left[\widehat{p}(k) + \widehat{p}(-k)^*\right] \tag{33}$$

$$\widehat{\xi} = \frac{1}{2i}\,\frac{(1+R)\omega}{|k|}\left[\widehat{p}(k) - \widehat{p}(-k)^*\right] \tag{34}$$

where the asterix represents the complex conjugate. Thus the problem is reduced to solving (31) which is a single complex evolution equation.

3 Normal Form Analysis

The nonlinear Schrödinger equation (NLS) is a conventional tool to predict the existence of bright and dark solitary waves, as well as the modulational instability for a quasi-monochromatic wave. 1D normal form analysis for the interfacial GC waves in deep water has been carried out by several authors, see Dias & Iooss [8] for example. In order to derive the cubic NLS, we define $X = \epsilon x$, $Y = \epsilon x$, $T = \epsilon t$, $\tau = \epsilon^2 t$ and $\Theta = kx + ly - \omega t$ where k and l are the wave numbers in x and y directions respectively and ω is the frequency. We substitute the ansatz

$$\begin{pmatrix}\eta\\ \xi\end{pmatrix} = \epsilon\begin{pmatrix}A(X,Y,T,\tau)\\ B(X,Y,T,\tau)\end{pmatrix}e^{i\Theta} + \epsilon^2\begin{pmatrix}A_1\\ B_1\end{pmatrix} + \epsilon^3\begin{pmatrix}A_2\\ B_2\end{pmatrix} + \cdots \tag{35}$$

into the system (26) and equate like powers of ϵ. It is worth mentioning that A_1, A_2 and B_1, B_2 include all the harmonic modes, i.e., $A_j = (\cdot)e^0 + (\cdot)e^{i\Theta} + (\cdot)e^{2i\Theta} + \cdots$. We assume that the carrier wave propagates only in the x-direction, namely we choose $l = 0$ and $k \neq 0$. The following formulae are applicable if necessary in the derivation

$$G_0\Big[f(X,Y)e^{i\Theta}\Big] = \Big[|k| - \frac{i\epsilon k}{|k|}\partial_X - \frac{\epsilon^2}{2|k|}\partial_{YY}\Big]f(X,Y)e^{i\Theta} + O(\epsilon^3) \tag{36}$$

$$\partial_t\Big[f(X,Y,T,\tau)e^{i\Theta}\Big] = \Big(- i\omega f + \epsilon f_T + \epsilon^2 f_\tau\Big)\, e^{i\Theta} + O(\epsilon^3) \tag{37}$$

$$\Delta\Big[f(X,Y)e^{i\Theta}\Big] = \Big(- k^2 f + \epsilon 2ikf_X + \epsilon^2 f_{XX} + \epsilon^2 f_{YY}\Big)\, e^{i\Theta} + O(\epsilon^3). \tag{38}$$

As the first step, terms are collected at $O(\epsilon)$ yielding the system

$$\begin{bmatrix} -i\omega & -\frac{|k|}{1+R} \\ 1-R+k^2 & -i\omega \end{bmatrix}\begin{pmatrix} A \\ B \end{pmatrix} = \begin{pmatrix} 0 \\ 0 \end{pmatrix}. \tag{39}$$

Since A and B are non-trivial, the determinant of the matrix should be zero. This yields the linear dispersion relation and the relation between A and B

$$\omega^2 = \frac{|k|}{1+R}\Big(1-R+k^2\Big), \qquad B = -\frac{i(1-R+k^2)}{\omega}A. \tag{40}$$

At $O(\epsilon^2)$, due to the dispersion relation, the linear system is also degenerate for the mode $e^{i\Theta}$. The solvability condition implies that A depends on T in an implicit way $A(X - c_g T, Y, \tau)$ and so does B, where c_g is called the group velocity which is defined by

$$c_g \triangleq \partial_k\omega = \frac{1-R+3k^2}{2\omega(1+R)}. \tag{41}$$

Finally the solvability condition for $O(\epsilon^3)$ gives the cubic NLS

$$iA_\tau + \frac{\frac{3k}{1+R} - c_g^2}{2\omega}\, A_{XX} + \frac{c_g}{2k}\, A_{YY} + \alpha\,|A|^2 A = 0 \tag{42}$$

where

$$\alpha = \frac{\omega k^2}{2}\Big[\frac{\frac{3}{2}k^2}{1-R+k^2} - 2 + \frac{2(1-R)^2(1-R+k^2)}{(1+R)^2(2k^2-1+R)}\Big]. \tag{43}$$

It is of particular interest to study the NLS coefficients at the minimum of the phase speed c_p, since it is easy to prove that at the minimum of c_p, the group velocity is equal to the phase velocity. Then wavepacket solitary waves may bifurcate from free stream at this minimum as long as the associated NLS is of

focussing type. At $k^2 = 1 - R$, c_p attains its minimum and the corresponding NLS reads

$$iA_\tau + \lambda_1 A_{XX} + \lambda_2 A_{YY} + \gamma \left|A\right|^2 A = 0 \tag{44}$$

with

$$\lambda_1 = \frac{\omega}{4(1-R)}, \quad \lambda_2 = \frac{\omega}{2(1-R)}, \quad \gamma = \frac{\omega(1-R)}{2}\left[\frac{4(1-R)^2}{(1+R)^2} - \frac{5}{4}\right]. \tag{45}$$

When $R = 0$ the expression (44) reduces to the classic NLS of the free-surface GC waves on deep water. It is clear that there is a critical value of the density ratio $R_c = \frac{21-8\sqrt{5}}{11} \approx 0.283$ below which the associated NLS is of focussing type, so that wavepacket solitary waves bifurcate from infinitesimal periodic waves only if $R < R_c$. However, Laget & Dias [13] computed numerically solitary waves for $R > R_c$, and Agafontsev *et al.* [1] derived the cubic-quintic NLS in the transition regime $R \approx R_c$, in which the quintic term is of focusing type, to explain why solitary waves can still exist even though the associated cubic NLS is of defocusing type.

4 Plane Waves

The numerical solutions to (31) are computed by using a Fourier spectral decomposition with a pseudo-spectral method: Hilbert transforms and derivatives are computed in Fourier space, while nonlinear terms are computed in physical space. In particular to compute 1D traveling waves, we expand the solution as

$$p(\theta) \;=\; \sum_{n=-N}^{N} a_n \, e^{i2\pi n\theta/L}, \qquad \theta = x - ct \tag{46}$$

where c is called the translating speed and L is the length of the computational domain. Since η is real and symmetric about $\theta = 0$ and ξ is real and anti-symmetric about $\theta = 0$, by the definition of $\widehat{p}$, a_n is real for arbitrary n. Substituting (46) into the governing equation (31) results in a series of nonlinear algebraic equations for the Fourier coefficients and the translating speed c. These unknowns are computed via a collocation method and Newton iterations. In most of the 1D calculations, 2048 Fourier modes are used in order to obtain sufficiently resolved traveling waves. The initial guess for the Newton algorithm is obtained by using the vanishing pressure method which was first presented in [19]. The basic idea is to add an artificial soliton-like forcing

$$P(\theta) = \delta e^{-\theta^2} \tag{47}$$

to the Bernoulli equation where δ is a given parameter. The amplitude of the solution is first increased by a continuation method. Then δ is progressively decreased to zero to obtain a solution without forcing. Once such a solution is

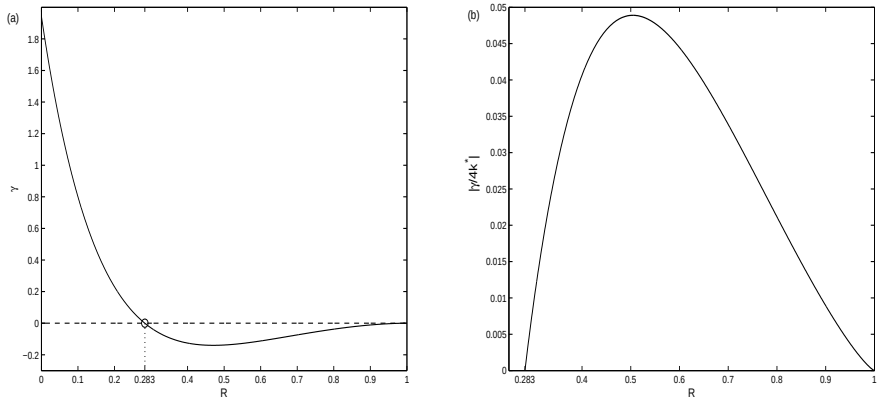

Figure 1: (a) Nonlinear self-interaction parameter γ whose expression is given in (45). (b) The coefficient $|\gamma/4k^*|$ given in (54).

found, other solitary waves on the branch can be computed via straightforward continuation methods.

For the 1D problem, the A_{YY} term should be neglected in the associated NLS equation (44). The nonlinear coefficient γ, whose expression is given in (45), is plotted in figure 1(a). When γ is close to zero, in the NLS analysis, the effects of the quintic nonlinearity are comparable to those of the cubic nonlinearity. In the small-amplitude limit, to rule out the effects due to the quintic nonlinearity in NLS, the absolute value of γ should not be very small. From figure 1(a), it is obvious that the ideal choice for the density ratio is $0 \leq R \leq 0.2$ in the subcritical regime, and $0.4 \leq R \leq 0.6$ in the supercritical regime. While in the transitional regime ($R \approx 0.283$), the modulations of wavepackets should be well described by a cubic-quintic NLS equation. And furthermore, in order to derive a correct cubic-quintic NLS equation, the high order terms omitted in (19) are clearly necessary (see [1] for details). It is noted that the derivation of the PDE model with sixth-order truncated kinetic energy is tedious and beyond the scope of this work.

4.1 Case I: $R < R_c$

We pick $R = 0.1$ as the typical density ratio in the subcritical regime. Figure 2(a) shows the speed-amplitude bifurcation diagram of the interfacial GC solitary waves, as obtained from the numerical solutions of the model (31) (solid line), the full potential flow (circles) and the leading-order of the NLS approximation (dashed line). The steady irrotational Euler flow is computed by conformal mappings and a boundary integral method with an auxiliary function joining the values of the potentials across the interface. The numerical scheme can be found for example in [13][18], and we omit the details in this paper. The NLS prediction is obtained by solving the 1D stationary NLS equation.

Substituting the ansatz $A = \rho(X)e^{i\Omega\tau}$ into the equation (44) with positive Ω, yields

$$A(X,\tau) = \sqrt{\frac{2\Omega}{\gamma}}\,\mathrm{sech}\left(\sqrt{\frac{\Omega}{\lambda_1}}\,X\right)e^{i\Omega\tau}. \tag{48}$$

Then it follows that

$$\eta(x,t) \approx 2\epsilon\sqrt{\frac{2\Omega}{\gamma}}\,\mathrm{sech}\left[\epsilon\sqrt{\frac{\Omega}{\lambda_1}}\,(x-c_g t)\right]\cos\left[k^*\left(x-c_p t+\frac{\epsilon^2\Omega}{k^*}t\right)+x_0\right]. \tag{49}$$

For $R = 0.1$, the coefficients are

$$k^* = 0.9487, \quad c_p = c_g = 1.3133 \triangleq c^*, \quad \lambda_1 = 0.3461, \quad \gamma = 0.8005. \tag{50}$$

In (49) x_0 is an arbitrary relative phase between the carrier wave and the envelop, which implies a continuous family of localized solutions characterized by the phase shift. However, only two types of solitary waves have been found for the irrotational Euler equation: depression waves (which have negative surface elevation at their center) corresponding to $x_0 = \pi$ and elevation waves (which have positive surface elevation at their center) corresponding to $x_0 = 0$. Typical profiles of depression and elevation solitary waves, using the model equation (31), are shown in figure 2(b)(c). One can further infer from the approximate solution (49) that close to the bifurcation point, the correction to the speed is $c^* - c \approx \frac{\Omega\epsilon^2}{k^*}$. This gives the leading-order speed-amplitude relation (dashed line in figure 2(a))

$$||\eta||_\infty \approx 2\epsilon\sqrt{\frac{2\Omega}{\gamma}} \approx \sqrt{\frac{8k^*}{\gamma}}\,(c^*-c)^{1/2}. \tag{51}$$

From the bifurcation diagram (figure 2(a)) we conclude that NLS is valid in the small-amplitude limit and for a very narrow range of values of the speed. The diagram also shows that both elevation and depression solitary waves bifurcate from infinitesimal periodic waves at the minimum of the phase speed when the density ratio is subcritical. On the other hand, the validation against the full Euler computation shows that our reduced model appears to be quantitatively accurate at relatively large amplitudes, far beyond the NLS-dominated regime. It should be remarked that we do not show the comparison between the full equation and the reduced model in figure 2(b)(c), since the error ($\approx 10^{-3}$) is too small to be perceived by naked eyes.

4.2 Case II: $R > R_c$

When the density ratio is in the supercritical regime, the analytical results of the defocusing NLS can guide our computation of small-amplitude waves near

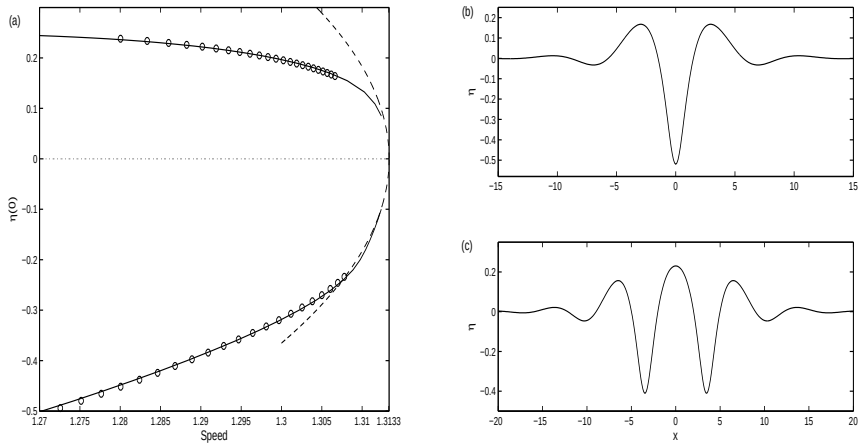

Figure 2: (a) One-dimensional speed-amplitude bifurcation diagram for both depression and elevation solitary waves together with the bifurcation point at 1.3133. The density ratio R is equal to 0.1 and therefore less than the critical ratio R_c. Solid curves, the model (31); circles, fully nonlinear potential flow; dotted lines, the leading-order NLS prediction. Typical free-surface profiles: a depression wave (b) with $\eta(0) = -0.52$ and $c = 1.2663$ and an elevation wave (c) with $\eta(0) = 0.2303$ and $c = 1.2848$. The solution to the full equations cannot be visually differentiated from these on this scale.

the bifurcation point. It is well-known that there is a family of dark solitary waves for the defocusing NLS given by

$$A = \sqrt{\frac{\Omega}{\gamma}}\ \tanh\left(\sqrt{-\frac{\Omega}{2\lambda_1}}\ X\right)\ e^{i\Omega\tau} \tag{52}$$

where Ω is an arbitrary negative constant. Hence viewed as solutions of the water wave problem, the leading-order expression for the surface displacement takes the form

$$\eta \approx 2\epsilon\sqrt{\frac{\Omega}{\gamma}}\tanh\left[\epsilon\sqrt{-\frac{\Omega}{2\lambda_1}}\,(x - c_g t)\right]\sin\left[k^*\left(x - c_p t + \frac{\epsilon^2\Omega}{k^*}t\right) + x_0\right]. \tag{53}$$

To simplify the problem, we only compute symmetric dark solitary waves in this paper. Therefore we take the phase shift $x_0 = 0$ or π. Steady dark solitary waves are characterized by a spatially local decrease in amplitude of a periodic train. In water wave problems, they approach a nonlinear train of Stokes waves in the far field. For this reason, the amplitude of a dark solitary wave is consistent with that of a Stokes wave, and the speed-amplitude dependence in the primitive variables can be approximately given by

$$c - c^* \ \sim\ \left|\frac{\gamma}{4k^*}\right|\ ||\eta||_\infty^2 \tag{54}$$

for the translating speed c slightly bigger than the minimum of the phase speed. We should emphasize that the coefficient $|\gamma/4k^*|$ is significant, since it is associated with the width of value of the translating speed for dark solitary waves or generalized solitary waves: the bigger the quantity is, the easier it is to study the bifurcation mechanism numerically. This quantity is plotted in figure 1(b), implying that the density ratio $R \in [0.4, 0.6]$ is a fine option. In order to keep both $|\gamma|$ and $|\gamma/4k^*|$ away from zero, we choose $R = 0.4$ as a typical density ratio in the supercritical case throughout this section (see figure 1). For $R = 0.4$, the constants in the associated NLS are respectively

$$k^* = 0.7746, \quad c_p = c_g = 1.0519 \triangleq c^*, \quad \lambda_1 = 0.3395, \quad \gamma = -0.1260. \tag{55}$$

Though the defocusing NLS predicts the non-existence of small-amplitude bright solitary waves, it does not rule out large-amplitude ones. In fact, finite-amplitude bright solitary waves, which are far beyond the weakly nonlinear regime, do exist in interfacial GC waves in deep water (see [13]). We begin with validating our reduced model (31) against the full potential flow equations by computing these bright solitary waves, since for these waves the accurate solutions to the full equation are available. Typical profiles of moderate-amplitude depression and elevation bright solitary waves, computed by the model equation (solid line) and irrotational Euler equations (dotted line), are shown in figure 4(a)(c). The relative maximum pointwise errors are about 0.03, from which we can conclude that the model (31) is still remarkably accurate even for large-amplitude interfacial GC waves in deep water.

We follow the branches of the depression and the elevation bright solitary waves by increasing the translating speed. As c increases and across the bifurcation point 1.0519, the finite-amplitude bright solitary wave starts to resonate with Stokes waves and therefore results in a generalized solitary wave which is composed by a localized midsection and non-decaying oscillatory tails. Typical profiles of the depression and the elevation generalized solitary waves are shown in figure 4(b)(d) respectively. We also change the domain size by adding $4\pi/k^*$, and redo the computation (see the dotted lines in figure 4(b)(d)). The resulting waves, with two periodic waves being added in the far field but without any noticeable change of the portion already obtained for smaller domain, strongly suggests the existence of actual generalized solitary waves as the domain size approaches infinity. When the speed further increases, corresponding to a decrease in the amplitude of the midsection, the tails of the generalized solitary wave grow and catch up with the central part in amplitude. Finally the generalized solitary waves merge in a branch of finite-amplitude Stokes waves. Overall, figure 3(a)(b) shows the bifurcation mechanism of the depression and the elevation branches respectively in the vicinity of the minimum of the phase speed when the density ratio is in the supercritical regime. It is clear that bright solitary waves (triangles on the left-hand side of the bifurcation point) bifurcate from generalized solitary waves (triangles on the right-hand side of the bifurcation point) which themselves bifurcate from finite-amplitude nonlinear periodic waves (circles). The bifurcation curve in figure 3(a) (circles+point-down triangles) is qualitatively similar to figure 1(a) in [14] for the free-surface GF waves

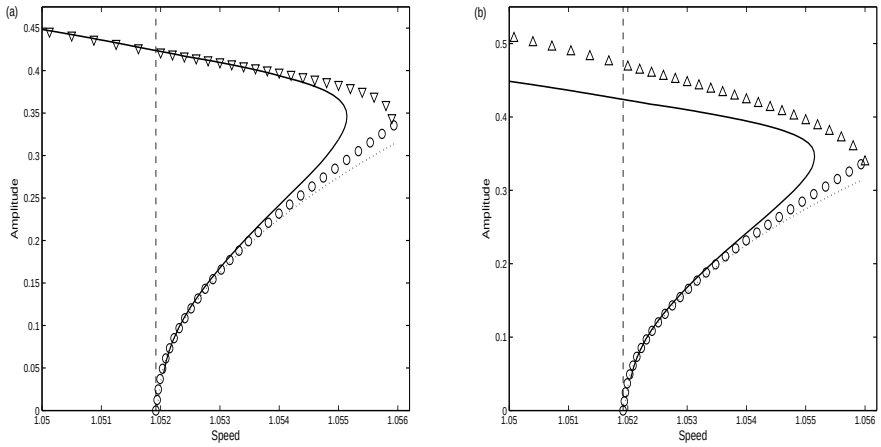

Figure 3: Speed-amplitude curves for traveling wave branches in the vicinity of the bifurcation point $c^* = 1.0519$ (which is shown by the vertical dashed line). The circles are the nonlinear periodic waves. The triangles correspond to the bright solitary ($c < c^*$) and the generalized solitary waves ($c > c^*$) for $R = 0.4$. There are two kinds of bright solitary waves: depression ones (triangles pointing downward in (a)) and elevation ones (triangles pointing upward in (b)). Also there are two branches of dark solitary waves shown in (a) and (b) with solid curves, at small amplitudes, to the two cases of (53) with $x_0 = 0$ and π respectively. The branch of waves with a minimum at $x = 0$ at small amplitude is shown in figure 6 (solid curves and dotted curves). Both branches of the steady dark solitary waves can be extended to $c < c^*$, where they are no longer dark solitons, but bright solitary waves. In both graphs, the dotted curve is the speed-amplitude curve predicted by the NLS equation (formulae (54)). The amplitude parameter in all cases is $[\max(\eta) - \min(\eta)]/2$.

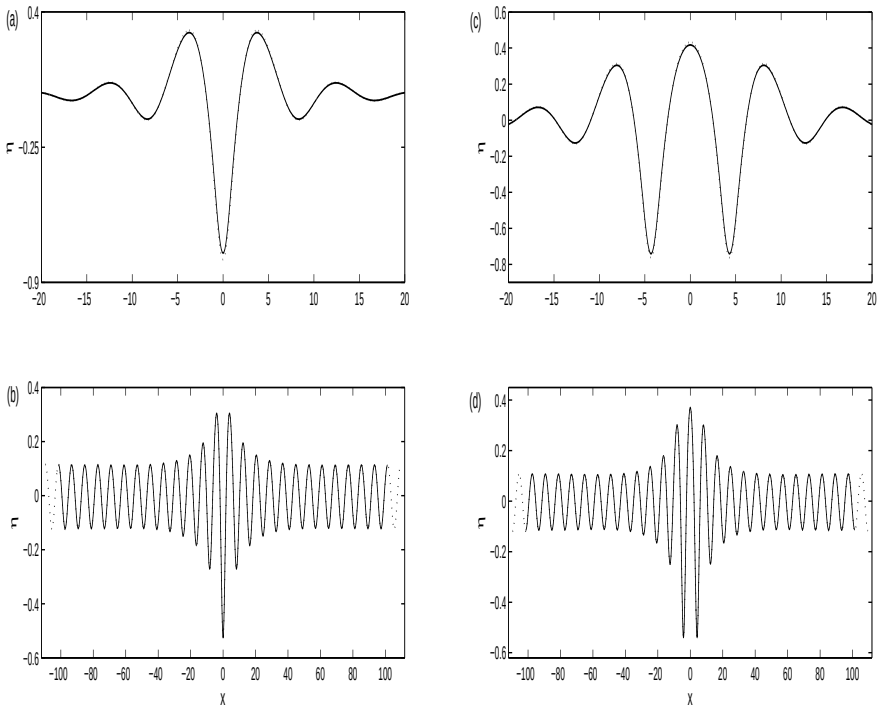

Figure 4: Examples of bright solitary waves and generalized solitary waves for $R = 0.4$. (a) depression bright solitary wave at $c = 1.04$: the result of the cubic model (solid curve) and the solution to the full Euler equation at the same speed (dotted curve) (the maximum difference between the model and full solutions is about 0.03); (b) depression generalized solitary wave computed with the cubic model at $c = 1.0526$: for the domain size $50\pi/k^*$ (solid line) and $54\pi/k^*$ (dotted line); (c) elevation bright solitary wave at $c = 1.044$: the profile computed with the model (solid curve) and the solution to the full Euler equation at the same speed (dotted curve) (the maximum difference between the model and full solutions is about 0.02); (d) elevation generalized solitary wave computed with the model at $c = 1.0526$: for the computing domain size $50\pi/k^*$ (solid curve) and $54\pi/k^*$ (dotted curve).

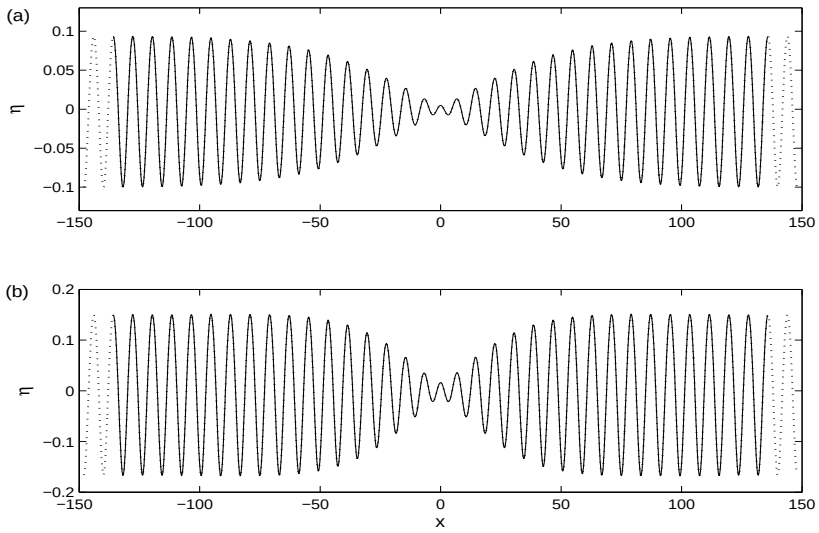

Figure 5: The comparison between the traveling dark solitary waves corresponding to the case of the positive pressure (positive δ in (47)) computed in a domain of the size $67\pi/k^*$ (solid curves) and that of the negative pressure (negative δ in (47)) computed in a domain with the size $73\pi/k^*$ (dotted curves). (a) $c = 1.0523$, (b) $c = 1.0529$.

on deep water. Nevertheless, the elevation branch has not been found in GF waves with Kirchhoff-Love elastic model. It is worth mentioning that the bright elevation solitary waves do exist in the GF waves if Toland's nonlinear elastic model is applied (see [9] for example). However in this case the full bifurcation diagram like that of figure 3(a)(b) is still not available due to numerical difficulties.

We next move on to the steady dark solitary waves which are predicted by the defocusing cubic NLS. As suggested in [15], in order to seek dark solitary waves for more primitive equations than cubic NLS, we should choose the domain with size $(2n+1)\pi/k^*$ to avoid the Stokes waves. Dark solitary waves are all found for $n = 22, 23, \cdots, 37$, which proves that our numerical method is robust. Since we try to compute symmetric steady dark solitary waves for equation (31), in the small-amplitude regime there are two possibilities for the middle phase: concave-up and concave-down. Unlike the free bright solitary wave whose phase is completely determined by the artificial pressure in vanishing pressure process, in the numerical computation, the phase of a dark solitary wave is determined by both the size of the computational domain and the phase of the pressure. Two domains with sizes L and $L + 4j\pi/k^*$ (j is an integer), forced with distinct signs (i.e. picking δ and $-\delta$ in (47)) results in dark solitary waves with different phases. On the other hand, if the domain sizes are L and $L + 2(2j+1)\pi/k^*$ respectively, forcing with different phases yields dark

solitary waves with the same phase. For instance, in figure 5 the solid lines are computed in a $67\pi/k^*$-long domain with positive forcing, while the dashed lines are computed in $73\pi/k^*$-long domain with negative forcing, but it turns out that they actually fall into the same branch.

The solid lines in figure 3 represent the speed-amplitude bifurcation diagrams for these two branches of the dark solitary waves. The dotted lines are the NLS approximation (54), which offers a good prediction for small amplitudes. Typical profiles along one branch are shown in figure 6(a)-(d). As the amplitude increases, the bifurcation curve exhibits a turning point, passing through which the solution transits from dark solitary waves to multi-hump generalized solitary waves, and evolves into multi-packet bright solitary waves after crossing over the bifurcation point from its right to its left. Since we compute waves in finite domains, the superpositions for the domain sizes $67\pi/k^*$ and $75\pi/k^*$ in figure 6(a)-(c) strongly suggest that more and more periodic waves can be added in the tails to approach the real dark and generalized solitary wavs.

5 Quasi-Planar Waves

We now turn our attention to 2D fully localized solitary waves. For $R < R_c$, the focusing NLS predicts the existence of these solutions since it supports fully localized stationary solutions. Substituting the ansatz $A = \frac{1}{\sqrt{\gamma}}\,\rho(r)\,e^{i\tau}$, where $r = \sqrt{\frac{X^2}{\lambda_1} + \frac{Y^2}{\lambda_2}}$, into (44), one obtains

$$\frac{d^2\rho}{dr^2} + \frac{1}{r}\frac{d\rho}{dr} + \rho^3 - \rho = 0 \tag{56}$$

with the boundary conditions

$$\frac{d\rho}{dr}\Big|_{r=0} = 0, \qquad \rho \to 0 \quad \text{as } r \to \infty. \tag{57}$$

The system (56)-(57) has countably many solutions characterized by the number of zeros of the solution. The first three solutions are plotted in figure 7. The first solution is called "ground state" which is positive definite. The second solution crosses zero once, the third one crosses zero twice, and so on.

For $R > R_c$, whilst the associated NLS becomes defocusing, the primitive irrotational Euler equation still has fully localized traveling wave solutions (in [16], Părău *et al.* have already presented one depression lump for $R = 0.485$). We show in this section that the reduced model (31) can also capture these features. We use the "ground state" to prepare the initial data for the Newton algorithm to seek solitary waves at speeds smaller than the minimum of the phase speed for $R < R_c$. Once such a solution is obtained, the fully localized traveling waves for $R > R_c$ can be computed via a straightforward continuation method using the density ratio as the continuation parameter. Similarly to the 1D case, there are two branches of lump solitary waves: depression and elevation. We present in figure 8 the interfacial profiles of two typical cases: an

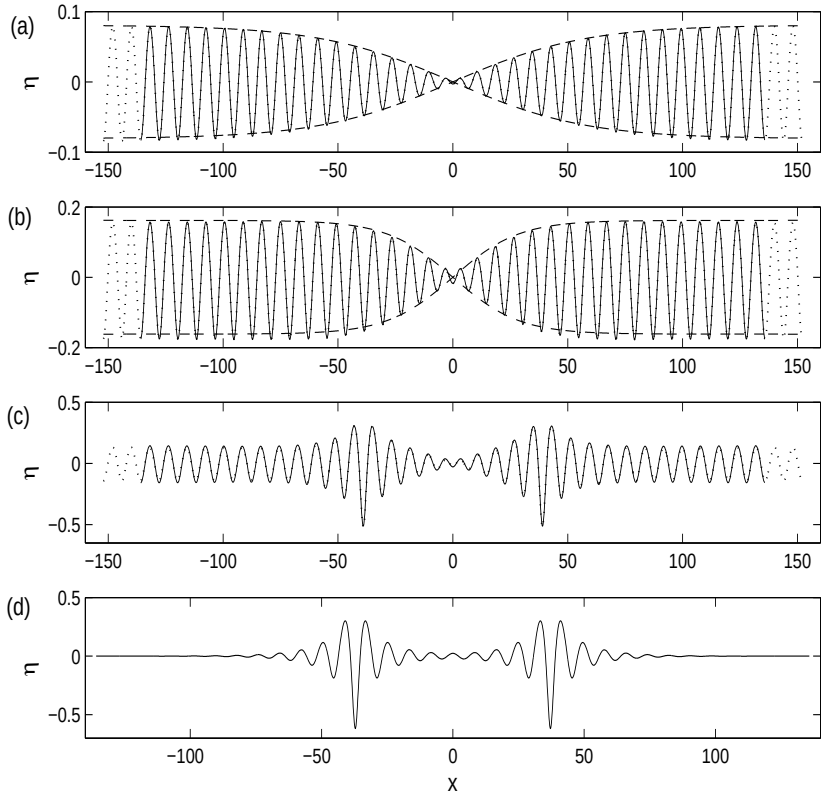

Figure 6: Traveling dark solitary waves corresponding to the branch of the concave-down midpoints. From (a-d), one moves along the branch by increasing the amplitude parameter from solutions whose envelope is well described by the dark soliton of NLS (dashed line) to a solution that resembles pairs of bright solitary waves with decaying oscillatory tails. The solid curves are computed in a $67\pi/k^*$-long domain, and the dotted curves are computed with the domain size of $75\pi/k^*$.

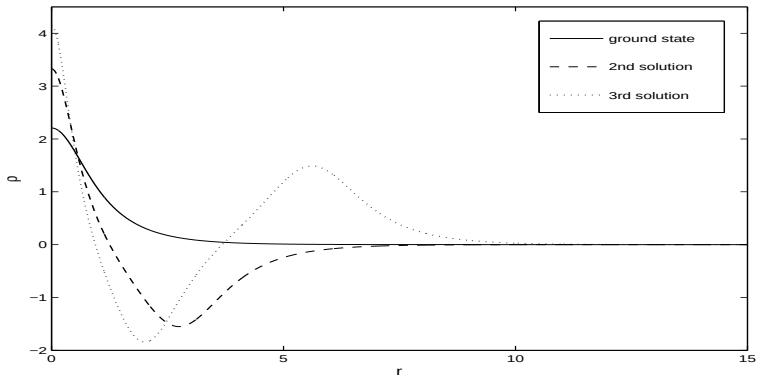

Figure 7: First three solutions to the boundary-value problem (56)-(57) that governs localized solutions of the envelope equation (44): ground state (solid curve), second solution (dashed curve) and third solution (dotted curve).

elevation lump for $R = 0.1$ and a depression lump for $R = 0.4$. As expected, these waves have decaying oscillatory tails in the direction of propagation and decay monotonically in the transversal direction.

Since the stationary NLS has countably many radial symmetric modes, the ground state is not the unique option for preparing the initial data in the Newton algorithm. In fact fully localized traveling waves constructed with the second solution of (56)-(57) have been found for $R = 0$ (see [20]). We generalize the result to the two-layer fluid system, and find that these high-energy solitary waves can even exist for supercritical density ratios. In figure 9 we show one example of such kind of solitary waves, which is initially computed with $R = 0.1$ using the second solution of (56)-(57), and then gradually continued to $R = 0.33$ by varying density ratio (256×128 grid points are used along the propagating and transverse directions respectively).

Similarly to the case of $R = 0$, high-energy solitary waves have complicated wave patterns and are unstable. Figure 10 shows the nonlinear evolution of a complex solitary waves constructed with the second solution of (56)-(57) for $R = 0.1$. The complicated structure is destroyed by the numerical noise and finally breaks up into four basic solitary waves corresponding to the "ground state". Time integration of the system is accomplished with the classic fourth-order Runge-Kutta method using an integrating factor. The computation is de-aliasing with a doubling of the Fourier modes.

6 Conclusion

The recent work on gravity-flexural waves on deep water stimulates further study of the interfacial gravity-capillary waves between two immiscible fluids of different densities. In this paper, we proposed a quantitative reduced model, derived from the quartic truncation of the kinetic energy in the Hamiltonian,

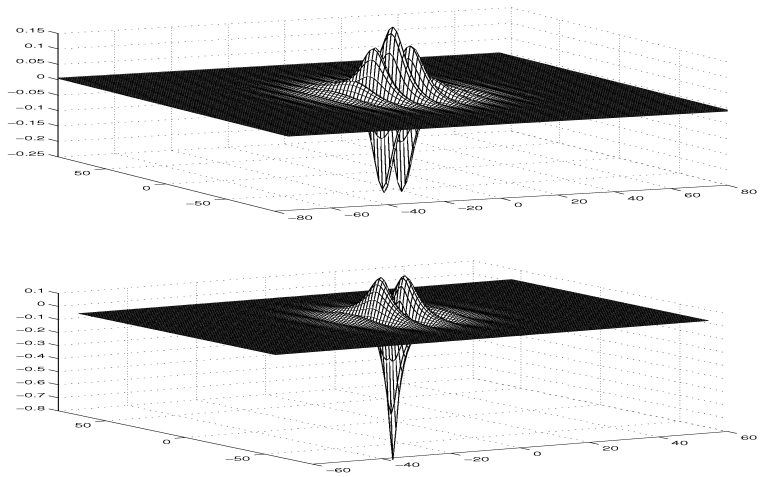

Figure 8: Typical interfaces of elevation and depression solitary waves for the model (31) for different densities. Top figure: $R = 0.1$, $c = 1.3068$ and $\eta(0,0) = 0.2175$; Bottom figure: $R = 0.4$, $c = 1.0414$ and $\eta(0,0) = -1.0971$.

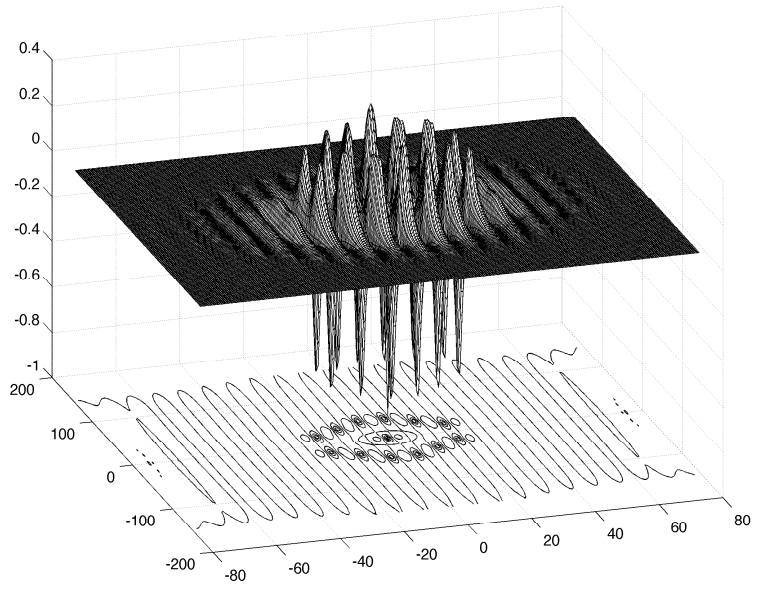

Figure 9: A typical profile of depression solitary waves corresponding to the second solution of the system (56)-(57) with $R = 0.33$, $c = 1.103$ and $\eta(0,0) = -0.8959$.

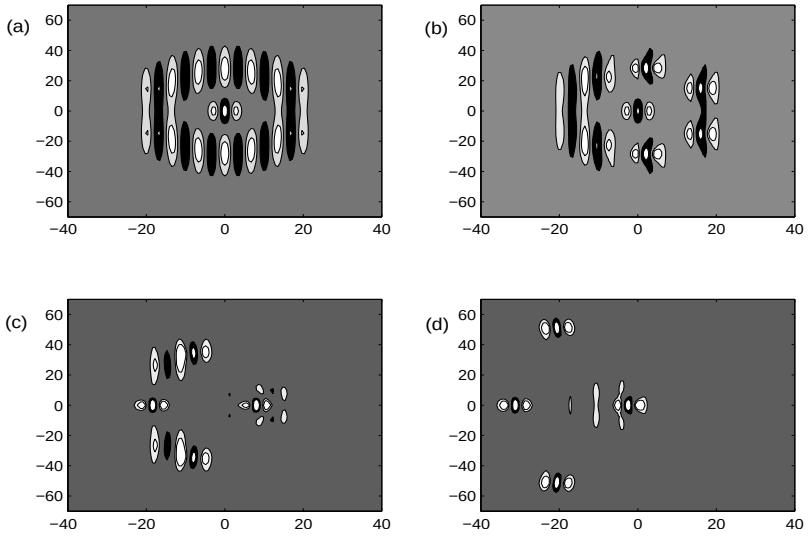

Figure 10: Instability of a high-energy depression solitary wave with $R = 0.1$, $c = 1.3057$ and $\eta(0,0) = -0.5217$. Snapshots of the evolution are shown at (a) $t = 0$, (b) $t = 448$, (c) $t = 660$, (d) $t = 900$. Four basic depression lumps corresponding to the "ground state" emerge from the complex behavior.

for the interfacial GC waves in deep water. This model equation enabled us to study the bifurcation mechanism in the vicinity of the minimum of the phase speed. Particular attention was paid to the case of relatively large density ratios, for which the defocusing nonlinear Schrödinger eqaution predicts the non-existence of solitary waves bifurcating from infinitesimal periodic waves. This weakly nonlinear analysis can only rule out the small-amplitude solitary waves. Nevertheless, large-amplitude waves do exist in the primitive potential flow equations. The presence of these solitary waves was first shown by Laget & Dias [13] using boundary integral methods. Using our model equation, we showed that these finite-amplitude bright solitary waves bifurcate from a branch of generalized solitary waves that itself bifurcates from finite-amplitude Stokes waves. Furthermore, steady dark solitary waves, which are predicted by the defocusing NLS, also exist in the right-hand side of the bifurcation point, but only in the small-amplitude regime. As the amplitude increases, the branches become a pair of generalized solitary waves and thereafter evolve into a pair of bright solitary waves after crossing the bifurcation point.

The model was also generalized to the 2D case in the spirit of the KP approximation. Fully localized lump solutions, which are constructed based on different solutions of the underlying NLS, were found even for relatively large density ratios.

It must be also mentioned that the Hamiltonian truncated model has its

limitation: it cannot be used to study very large-amplitude waves or waves with complicated structures, like overhanging waves. While they are beyond the scope of this paper, we believe that the stability properties of interfacial solitary waves for both 1D and 2D cases, and the fate of the branch of the 1D steady dark solitary waves are of particular interest, and merit further study using the primitive irrotational Euler equation.

Acknowledgements

Z. W. and J.-M. V.-B acknowledge support from EPSRC grant EP/J019569/1.

References

[1] D.S. Agafontsev, F. Dias, and E.A. Kuznetsov, Deep-water internal solitary waves near critical density ratio, *Physica D* 225:153–168 (2007).

[2] B. Akers and P.A. Milewski, A model equation for wavepacket solitary waves arising from capillary-gravity flows, *Stud. Appl. Math.* 122:249–274 (2009).

[3] T.B. Benjamin and T.J. Bridges, Reappraisal of the Kelvin-Helmholtz problem. Part 1: Hamiltonian structure, *J. Fluid Mech.* 333:301–325 (1997).

[4] T.J. Bridges and N.M. Donaldson, Secondary criticality of water waves. I. Definition, bifurcation and solitary waves, *J. Fluid Mech.* 565:381–417 (2006).

[5] W. Craig, Non-existence of solitary water waves in three dimensions, *Phil. Trans. R. Soc. Lond. A* 360:2127–2135 (2002).

[6] W. Craig and M.D. Groves, Normal forms for wave motion in fluid interfaces, *Wave Motion* 31:21–40 (2000).

[7] R. Coifman and Y. Meyer, Nonlinear harmonic analysis and analytic dependence, *Proc. Symp. Pure Math.* 43:71–78 (1985).

[8] F. Dias and G. Iooss, Capillary-gravity interfacial waves in infinite depth, *Eur. J. Mech. B/Fluids* 15:367–393 (1996).

[9] P. Guyenne and E.I. Părău, Computations of fully nonlinear hydroelastic solitary wave on deep water. *J. Fluid Mech.* 713:307–329 (2012).

[10] K.R. Helfrich and W.K. Melville, Long nonlinear internal waves, *Annu. Rev. Fluid Mech.* 38:395–425 (2006).

[11] B. Kim and T.R. Akylas, On gravity-capillary lumps. Part 2. Tow-dimensional Benjamin equation, *J. Fluid Mech.* 557:237–256 (2006).

[12] E.A. Kuznetsov, M.D. Spector, and V.E. Zakharov, Surface singularities of ideal fluid, *Phys. Lett. A* 182:387–393 (1993).

[13] O. Laget and F. Dias, Numerical computation of capillary-gravity interfacial solitary waves, *J. Fluid Mech.* 349:221–251 (1997).

[14] P.A. Milewski, J.-M. Vanden-Broeck, and Z. Wang, Hydroelastic solitary waves in deep water, *J. Fluid Mech.* 679:628–640 (2011).

[15] P.A. Milewski, J.-M. Vanden-Broeck, and Z. Wang, Steady dark solitary flexural gravity waves, *Proc. R. Soc. A* 469:20120485 (2013).

[16] E.I. Părău, J.-M. Vanden-Broeck, and M.J. Cooker, Three-dimensional gravity and gravity-capillary interfacial flows, *Math. Comp. Simu.* 74:105–112 (2007).

[17] C. Sulem and P.L. Sulem, *The nonlinear Schrördinger equation: self-focusing and wave collapse*, Applied Mathematical Sciences, Vol. 139, Springer-Verlag, New York (1999).

[18] J.-M. Vanden-Broeck, Numerical calculation of gravity-capillary interfacial waves of finite amplitude, *Phys. Fluids* 23:1723–1726 (1980).

[19] J.-M. Vanden-Broeck and F. Dias, Gravity-capillary solitary waves in water of infinite depth and related free-surface flows, *J. Fluid Mech.* 240:549–557 (1992).

[20] Z. Wang and P.A. Milewski, Dynamics of gravity-capillary solitary waves in deep water, *J. Fluid Mech.* 708:480–501 (2012).

[21] V.E. Zakharov, Stability of periodic waves of finite amplitude on the surface of a deep fluid, *J. Appl. Mech. Tech. Phys.* 2:190–194 (1968).

University College London

University College London

Unviersity College London

(Received)